

Breakdown of diameter selectivity in a reductive hydrogenation reaction of single-walled carbon nanotubes

Katalin Nemeth^a, Emma Jakab^b, Ferenc Borondics^{a,1}, Hajnalka M. Tóhádi^a,
Áron Pekker^{a,2}, Mónika Bokor^a, Tamás Verebélyi^a, Kálmán Tompa^a,
Sándor Pekker^{a,c}, Katalin Kamarás^{a,*}

^a*Institute for Solid State Physics and Optics, Wigner Research Centre for Physics,
Hungarian Academy of Sciences, P.O. Box 49, H 1525 Budapest, Hungary*

^b*Institute of Materials and Environmental Chemistry, Research Centre for Natural
Sciences, Hungarian Academy of Sciences, P.O. Box 286, H 1519 Budapest, Hungary*

^c*Óbuda University, Doberdó út 6, H 1034 Budapest, Hungary*

Abstract

Reductive hydrogenation was applied to two types of single-walled carbon nanotubes with different diameter range. Alkali metal intercalation, followed by reaction with methanol, led to hydrogenated products. Both yield and selectivity of this reaction showed strong dependence on diameter, contrary to expectation based on simple curvature effects. The observed yield, as detected by thermogravimetry-mass spectrometry and ¹H-NMR, is drastically reduced in small-diameter tubes where the alkali dopant does not reach the inside of the bundles. Wide range optical transmission measurements were employed to determine the selectivity and indicate that besides higher yield, lower diameter selectivity occurs above a critical diameter.

Keywords: carbon nanotubes, functionalization, bundles, diameter selectivity

*Corresponding author

Email address: kamaras.katalin@wigner.mta.hu (Katalin Kamarás)

¹Present address: Soleil Synchrotron, BP 48, L'Orme des Merisiers, 91192 Gif sur Yvette Cédex, France

²Present address: Center for Nanoscale Science and Engineering, Departments of Chemistry and Chemical & Environmental Engineering, University of California, Riverside, CA 92521, U.S.A.

Preprint submitted to Chemical Physics Letters

November 9, 2014

1. Introduction

Chemical modification of carbon nanotube surfaces by sidewall reactions is important for any application where further chemical bonding or increase in solubility is desired. Nanotube chemistry, however, constitutes many challenges compared to conventional organic chemistry methods: pristine nanotubes are insoluble in most solvents, and solid samples contain bundles of many tubes, held together by van der Waals forces. To increase contact between reactants and the tube surface, exfoliation and solubilization are required. These unique characteristics also mean that other factors than the chemical properties have to be taken into account when predicting the yield of a chemical reaction.

Reductive reactions, where the first step consists of charging the reactants, are especially well suited for exfoliation. Several types of modified Birch reduction are found in the literature [1, 2, 3, 4], using ammonia, tetrahydrofuran and ethylenediamine as solvent. The first step is electron transfer onto the nanotubes, where repulsion between the resulting negatively charged "supermolecules" helps exfoliation and promotes further reactions. Similar processes can happen in alkali metal intercalated graphite compounds [5], resulting in partially hydrogenated graphite [6].

Following graphite intercalation compounds[5], nanotube exfoliation possibilities and processes [7, 8], we applied direct reduction by intercalating alkali metals into carbon nanotube bundles. Based on these results and the rather similar reactivity of graphite and carbon nanotubes, we expected alkali metal intercalation to exfoliate and reduce nanotube bundles. By this method, the step of carbanion formation during the reductive modification could be separated in space and time from the attachment of the functional group (unlike other Birch-type reactions) [9].

Adding alkali metals to carbon nanotubes in excess, over time a saturation concentration (about KC_9 for potassium) is reached [10]. A stable phase (with composition KC_{27} determined by XPS) is formed in a few minutes at 180 °C. Structural characterization of K- and Cs- doped SWNTs by X-ray diffraction and electron microscopy proved that the alkali ions are attached to the tube surfaces, increasing the bundle size, instead of being encapsulated into the tubes [11]. Sidewall functionalization of the nanotubes can proceed from the doped phase by electrophilic addition.

1
2
3
4
5 The general selectivity of sidewall reactions in nanotubes is believed to be
6 determined principally by structural strain caused by π -orbital misalignment
7 on the curved surface [12], resulting in higher reactivity of smaller diam-
8 eter tubes. Considering one nanotube, these features determine diameter
9 selectivity thermodynamically. Taking into account, however, that realistic
10 nanotube samples consist of bundles, there are other important phenomena
11 that must be considered, such as kinetics, steric effects and energetics of all
12 processes and intermediate products in a reaction.
13
14

15 The effect of bundling is an unusual and exciting feature of nanotube
16 properties and reactions, and has been subject of many previous investi-
17 gations. One especially relevant to reductive reactions is the careful and
18 detailed study by Kukovecz et al. [13] on the first step of these reactions,
19 the doping of bundled nanotubes, using resonant Raman spectroscopy and
20 conductivity measurements. They found that in HiPco tubes a minimum in
21 doping level appears at around 1.1 nm. They explained their findings by tak-
22 ing into account the morphology of the bundles, and calculated the required
23 relative lattice expansion as a function of the size of the intertube channels
24 in the bundles, which is proportional to the tube diameter. According to
25 their calculations, above 1.3 nm tube diameter, there is no need for lattice
26 expansion for incorporating K^+ ions. At low diameters, however, another
27 effect has to be taken into account, the increasing stacking interaction in
28 the bundle, inversely proportional to tube diameter [14]. This latter effect
29 competes with the increasing reactivity at higher curvature.
30
31
32
33

34 In this paper, we describe the results of intercalation of single-walled car-
35 bon nanotubes (SWNTs) by alkali metals, followed by electrophilic addition
36 of protons to yield hydrogenated products. We used two types of commercial
37 nanotube samples as starting materials, with different diameter range, above
38 and below 1.2 nm. As dopant ions we used potassium and rubidium, similar
39 in chemical properties but differing in size, in order to reach two extreme
40 combinations (potassium with the larger diameter tubes, rubidium with the
41 smaller ones). The products were investigated by thermogravimetry-mass
42 spectrometry (TG-MS), 1H -NMR spectroscopy, Raman spectroscopy and
43 wide range optical transmission spectroscopy to obtain detailed information
44 about the reactivity through the composition, thermal and optical properties
45 of the samples, with special attention to diameter selectivity. We find that
46 above a critical intertube channel/ionic radius ratio, the yield increases and
47 becomes independent of diameter.
48
49
50
51
52
53
54
55
56
57
58
59
60
61
62
63
64
65

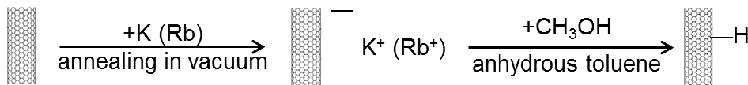


Figure 1: Direct reduction of single-walled carbon nanotubes by intercalating potassium

Table 1: Specific parameters of nanotube reactions.

Nanotube	Diameter range (nm)	Mean diameter (nm)	Dopant	Ionic radius (nm)	r_D/d_{NT}
P2	1.2-1.7	1.60	K	0.138	0.086
CoMoCat	0.57-1.17	0.90	Rb	0.152	0.169

2. Experimental

Two types of commercially available single-walled carbon nanotubes, differing in average diameter, were used: P2 by Carbon Solutions and CoMoCat CG by SouthWest NanoTechnologies. In order to reach two extremes of the dopant radius to diameter ratio r_D/d_{NT} , P2 tubes were doped with potassium and CoMoCat tubes with rubidium. Parameters of the reactants are summarized in Table 1. Calculated intertube channel radii from the mean diameter values in Table 1, according to Ref. [13], are 0.15 nm for P2 and 0.096 nm for CoMoCat. Comparing these values with the dopant radii, the K/P2 combination represents a case where the channels can easily accommodate the dopant ions, whereas for Rb/CoMoCat the ionic radius of the dopant by far exceeds the intertube channel radius. This difference is expressed in the r_D/d_{NT} ratio, given in the last column of Table 1.

The hydrogenation method, which was inspired by graphite intercalation compounds, is described below and shown in Figure 1.

In the case of P2, about 100 mg of as-received SWNT was first annealed in dynamic vacuum (at 10^{-6} mbar) at 250 °C for 12 hours, followed by transfer into an argon dry box. Potassium was added in a glass vial, keeping the SWNT-K molar ratio 4:1. The glass vial was sealed on a vacuum line. Annealing at 200 °C for 12 hours was enough for potassium to intercalate the nanotubes. Intercalation was indicated by the copper/gold color of the sample. Subsequently, the sample was put into a Schlenk-type flask with a funnel. 40 ml anhydrous toluene (Sigma-Aldrich, cryo-distilled from Na-K alloy) was added to the flask and 20 ml into the funnel. Toluene was used as a totally aprotic solvent to avoid side reactions with any other H source, and to control alkali metal atoms to intercalate the nanotubes and

1
2
3
4
5 not to dissipate in the solvent. Sonication was applied for 15 minutes to
6 enhance the intercalation process. Next, 5 ml methanol (Sigma-Aldrich,
7 used as received) was filled carefully into the funnel. Methanol was added
8 dropwise into the flask during sonication. Sonication was continued for 2
9 more hours, and the mixture was left overnight. The sample was filtered on
10 a *Millipore* nylon membrane filter (0.1 μm pore size), washed with ethanol,
11 1:3 HCl:H₂O, distilled water, ethanol and acetone. Finally it was dried in
12 dynamic vacuum at 200 °C for 12 hours. The product obtained this way
13 was transferred back into the dry box. The whole process described above,
14 except prior annealing, was repeated two more times in order to investigate
15 whether it is possible to improve the degree of hydrogenation by applying
16 successive steps. For CoMoCat, rubidium was used instead of potassium as
17 intercalating agent, in order to achieve larger bundle expansion [15]. The
18 main products of these reactions are hydrogenated nanotubes, but there are
19 side reactions, such as hydrogen evolution, when attachment of H to the
20 nanotube is kinetically hindered, or when the unreacted alkali metal reduces
21 methanol directly.

22
23
24
25
26
27 Reference samples were made of pristine P2 and CoMoCat by perform-
28 ing the same steps as with the hydrogenation reactions (initial annealing,
29 annealing in sealed glass tube, addition of methanol, washing, annealing in
30 dynamic vacuum), *except addition of alkali metal*.

31
32 Thermogravimetry-mass spectrometry (TG-MS) measurements were used
33 to determine the composition of the samples, particularly the H content. The
34 main purpose of the measurement is the quantitative determination of the
35 decomposition products as a function of temperature. Mass change with
36 temperature is directly measured by a Perkin-Elmer TGS-2 thermobalance
37 and a HIDEN HAL 2/301 PIC quadrupole mass spectrometer. 2-4 mg sample
38 in a Pt vessel was heated up to 800 °C with 20 °C/min rate in Ar atmosphere.
39 A portion of the volatile products was introduced into the mass spectrometer
40 (operated at 70 eV in electron impact ionization mode) through a heated
41 glass-lined steel capillary. Ion intensities were normalized to ³⁸Ar isotope of
42 the carrier gas to eliminate errors resulting from the shift in MS intensities.
43 To measure hydrogen (m/z 2), a calibration with TiH₂ is necessary. During
44 the measurements, signals of 16 ions were followed.

45
46
47
48 Wide line ¹H-NMR measurements and data acquisition were accomplished
49 by a Bruker AVANCE III NMR spectrometer at the frequency of 82.4 MHz
50 with a stability better than $\pm 10^{-6}$. The inhomogeneity of the magnetic field
51 was 2 ppm. Free induction decays (FIDs) were measured at room temper-
52
53

1
2
3
4
5 ature. Known amounts (weight) of the nanotubes (typically 7-15 mg) and
6 adamantane (99+%, Sigma-Aldrich) were put in Teflon capsules. The FID
7 measured on the empty capsule was subtracted from the FID of the actual
8 capsuled sample to correct for background. The amplitude of the FID at
9 zero time is proportional to the number of ^1H nuclei in the sample [16]. The
10 first 9-10 μs of the FID was lost in the dead time of the spectrometer. The
11 observed FIDs were extrapolated back to zero time by fitting Gaussian func-
12 tions to obtain its zero-time amplitude. The FID of adamantane was used for
13 calibration in calculating the hydrogen concentrations. There were residual
14 magnetic catalyst particles in the samples (typically 2-5 w/w%), but they
15 did not disturb the measurement significantly [3].

16 Raman spectra were taken by a Renishaw 1000B spectrometer using 785
17 nm excitation wavelength, with 4 cm^{-1} spectral resolution. The laser power
18 was kept sufficiently low in order to exclude heat damage.

19 Wide range optical transmission measurements were carried out on self-
20 supporting thin films made of the samples [17]. Transmission data between
21 $25\text{-}52500\text{ cm}^{-1}$ were recorded, by a Bruker IFS 66v/s FT-IR instrument in
22 the far and mid-infrared region, a Bruker Tensor37 in the near infrared, and
23 a Jasco v550 spectrometer in the visible and UV. Optical conductivity data
24 were obtained by performing Kramers-Kronig (KK) transformation on the
25 transmission data (atomic force microscopy was used to determine sample
26 thickness for KK calculations) [18]. Optical conductivity spectra were fit-
27 ted by the Drude-Lorentz model. After subtracting the background and all
28 other peaks related to transitions between different Van Hove singularities,
29 we obtained the contribution of the specific peaks [19].

30 31 32 33 34 35 36 37 38 **3. Results and discussion**

39 Raman spectra were recorded in order to detect changes in the D/G
40 mode intensity ratio. The increase in D/G ratio indicates the presence of
41 more defects in the nanotube sidewall. This is characteristic of functionalized
42 nanotubes, in which the sp^3 carbon atoms in the sidewalls act as defects [20,
43 21]. Raman spectra of both samples are shown in Figure 2. Each spectrum is
44 normalized to the G band to be comparable. The D/G ratio increases upon
45 functionalization, but the change cannot be used for quantitative estimation
46 of the sidegroup content, because of the complicated origin of the D band
47 [22]. To determine the hydrogen content more precisely, TG-MS and NMR
48 spectrometry were employed.

1
2
3
4
5
6
7
8
9
10
11
12
13
14
15
16
17
18
19
20
21
22
23
24
25
26
27
28
29
30
31
32
33
34
35
36
37
38
39
40
41
42
43
44
45
46
47
48
49
50
51
52
53
54
55
56
57
58
59
60
61
62
63
64
65

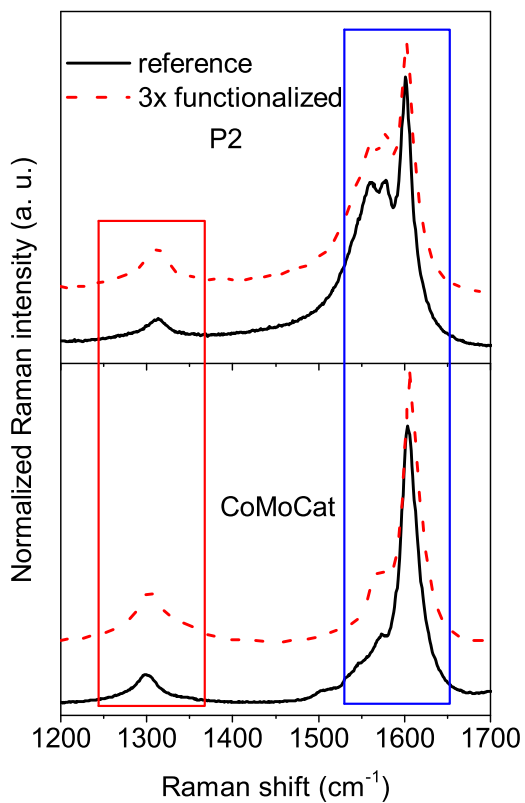


Figure 2: Raman spectra of the two samples (excitation wavelength: 785 nm) before functionalization (reference) and after three functionalization steps. Red frame: D modes; blue frame: G modes. Each spectrum is normalized to the G mode. Increasing D/G ratio indicates sidewall hydrogenation.

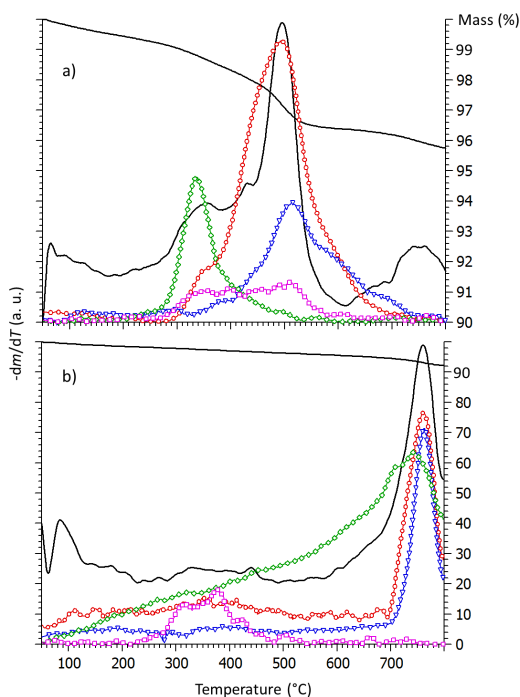


Figure 3: Typical TG-MS curves of the samples. a) P2, b) CoMoCat. Black solid lines in both graphs represent mass loss and its derivative, respectively. Notations for graph a): (red circles) m/z 2 hydrogen; (blue triangles) m/z 16 methane; (green diamonds) m/z 31 methanol; (magenta squares) m/z 92 toluene. For graph b): (red circles) m/z 2 hydrogen; (blue triangles) m/z 28 CO; (green diamonds) m/z 44 CO₂; (magenta squares) m/z 92 toluene, where m is the atomic mass and z the atomic number.

Results of the TG-MS measurements are shown in Figure 3 and Table 2. In case of the CoMoCat tubes the H-content was so small that the hydrogen evolution peak faded into the background, therefore the exact temperature of hydrogen evolution could not be determined.

The degrees of hydrogenation measured by NMR follow the same trend as TG-MS: the value obtained for CoMoCat is smaller than that for P2. Both methods proved the presence of hydrogen, although they have not yet been systematically compared. Since NMR measures the total hydrogen content in the sample, we consider the TG-MS method as yielding more precise quantitative results of hydrogen with chemical bonding to the nanotube walls. The hydrogen content of the products formed from P2 is between 2-4 at%. In contrast, in smaller diameter CoMoCat samples, where Rb was used as

Table 2: H content and thermal stability of the samples. NMR data are related to the samples with the highest degree of hydrogenation measured by TG-MS. H content determined by NMR are corrected with the H content of the reference samples to correct with the H content of other H containing materials (toluene etc.).

Sample	T_{\max} [H] ($^{\circ}\text{C}$)	H /100C (TG-MS)			[H] (mmol/g)	H /100C
		1	2	3	(NMR)	(NMR)
P2	350	2.17	2.41	3.61	4.63 ± 0.27	5.6
CoMoCat	–	<1	<1	<1	2.39 ± 0.15	2.9

intercalating alkali metal, the degree of hydrogenation is very small. This fact is in good agreement with previous studies [23, 24].

From special features in the optical spectra, conclusions can be drawn about the reactivity of the starting material [21, 25, 26]. The energy of the interband transitions (or likewise, transitions between excitonic levels close to the band edge) scales with the inverse diameter of the respective tubes. The width of the peaks in the optical spectra reflects mainly the diameter distribution of peaks in the sample, and therefore the change in shape upon a chemical reaction reflects the change in distribution between the starting material and the product. The most precise procedure to extract these changes from solid-state spectra is to compare the optical conductivity. This quantity is additive when several independent processes are involved (like light absorption by different nanotubes) and its calculation takes into account the reflectance at the interfaces, which can heavily influence the optical density calculated from transmittance [18]. The model we used [19] involves a reliable background correction and results in curves reflecting one type of transition across various diameter samples. The advantage of using optical spectra to determine changes in diameter distribution over Raman spectroscopy is that there is no resonance process which prefers certain nanotubes over others with selective increase in the scattering intensity.

Figure 4 compares the change in optical conductivity upon hydrogenation in the spectral regions connected to the first (S_{11}) and second (S_{22}) transitions between semiconducting nanotube energy levels. The curves shown are those of the products with the highest hydrogen content, obtained after three steps of hydrogenation. Intensity loss due to hydrogenation is independent of frequency in P2, and increases with increasing frequency in CoMoCat.

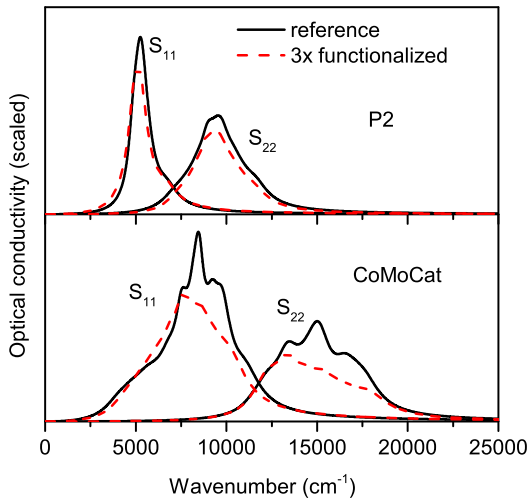


Figure 4: The effect of hydrogenation on the first (S_{11}) and second (S_{22}) semiconducting interband transitions in the optical spectra. In both cases, the reference sample and the product with the highest hydrogen content are shown.

This change indicates that the reactivity is determined by the penetration of the dopant into the bundles: in P2, the intensity decreases independently of frequency, whereas in CoMoCat the inverse diameter dependence returns. In the latter case, the effect of the bundles seems to disappear, since the alkali atoms will cover only the bundle surface. This effect results in much lower yield but "normal" diameter selectivity, determined by the curvature of the nanotubes.

In the first approximation, intercalation should proceed according to the first transition energy (S_{11} in semiconducting nanotubes). Since this quantity scales inversely with diameter, the first reaction step would be more probable for higher diameter tubes. These two opposite trends (that of the ionic intercalation step and the chemical reaction, described above) determine the rate of the reaction and therefore it is not surprising that it is not monotonous with diameter. An added complication arises because the intercalation happens inside bundles, introducing additional factors. Since intercalation into bundles formed by larger diameter tubes is less hindered, these bundles will be more reactive, both by their larger electron density and better availability for reactant molecules [13]. Above the diameter limit estimated (1.3-1.5 nm), where the intertube channels are wider than the ionic radius, potassium intercalation becomes unhindered and because of high availability for reactant

1
2
3
4
5 molecules (loosened bundles) very little diameter selectivity can be detected.
6 This is the case of the K/P2 sample. As the channels become narrower com-
7 pared to the intercalant ion, intercalation becomes more and more hindered
8 until it will be energetically totally unfavorable. In this case (Rb/CoMoCat),
9 electron transfer is possible only at the surface of the bundles, which causes
10 a drastic lowering in availability of tubes [23]. Below the transitory diameter
11 range the diameter selectivity will be determined by the chemical reaction,
12 favoring higher curvature, as observed in the case of CoMoCat.
13
14

15 We did not address the question of selectivity between metallic and semi-
16 conducting tubes; as in the first intercalation step all the tubes acquire metal-
17 lic character due to doping with charge carriers from the alkali metal [27],
18 we do not consider this effect significant.
19
20

21 **4. Conclusion**

22
23 We have synthesized hydrogenated single-walled carbon nanotubes by
24 alkali metal intercalation and subsequent reaction with methanol. By using
25 two samples with widely different diameter distributions (P2 and CoMoCat),
26 we could investigate diameter selectivity. We have revealed the role of alkali
27 metal intercalation in diameter selectivity of similar reductive reactions. The
28 results are in agreement with previous studies on alkali metal intercalated
29 nanotubes. We demonstrated that factors other than structural strain must
30 be considered in reactions that are driven in not totally homogeneous media
31 such as bundled nanotubes. For practical purposes of nanotube chemistry,
32 our results explain why a nanotube sample with low average diameter can
33 in fact produce lower yield in chemical reactions than nanotubes above a
34 critical diameter limit.
35
36
37
38
39

40 **5. Acknowledgement**

41
42 This research was funded by the Hungarian National Science Fund (OTKA)
43 under grant No. 105691.
44
45

- 46 [1] Y. Chen, R. C. Haddon, S. Fang, A. M. Rao, P. C. Eklund, W. H.
47 Lee, E. C. Dickey, E. A. Grulke, J. C. Pendergrass, A. Chavan, B. E.
48 Haley, R. E. Smalley, Chemical attachment of organic functional groups
49 to single-walled carbon nanotube material, *J. Mater. Res.* 13 (1998)
50 2423–2431.
51
52
53

- 1
2
3
4
5 [2] S. Pekker, J.-P. Salvetat, E. Jakab, J.-M. Bonard, L. Forró, Hydro-
6 genation of carbon nanotubes and graphite in liquid ammonia, *J. Phys.*
7 *Chem. B* 105 (2001) 7938–7943.
8
9 [3] F. Borondics, M. Bokor, P. Matus, K. Tompa, S. Pekker, E. Jakab,
10 Reductive functionalization of carbon nanotubes, *Fullerenes, Nanotubes*
11 *and Carbon Nanostructures* 13 (2005) 375–382.
12
13 [4] F. Borondics, E. Jakab, S. Pekker, Functionalization of carbon nan-
14 otubes via dissolving metal reductions, *Journal of Nanoscience and Nan-*
15 *otechnology* 7 (2007) 1–9.
16
17 [5] M. S. Dresselhaus, G. Dresselhaus, Intercalation compounds of graphite,
18 *Advances in Physics* 30 (1981) 139–326.
19
20 [6] D. E. Bergbreiter, J. M. Killough, Reactions of potassium-graphite, *J.*
21 *Am. Chem. Soc.* 100 (1978) 2126–2134.
22
23 [7] A. Dailly, J. W. L. Yim, C. C. Ahn, E. Miura, R. Yazami, B. Fultz,
24 Purification of carbon single-wall nanotubes by potassium intercalation
25 and exfoliation, *Appl. Phys. A* 80 (2005) 717–722.
26
27 [8] O. Tanaïke, O. Kimizuka, N. Yoshizawa, K. Yamada, X. Wang, H. Ha-
28 tori, M. Toyoda, Debundling of SWCNTs through a simple intercalation
29 technique, *Electrochemistry Communications* 11 (2009) 1441–1444.
30
31 [9] D. Voiry, O. Roubeau, A. Pénicaud, Stoichiometric control of single
32 walled carbon nanotubes functionalization, *J. Mater. Chem.* 20 (2010)
33 4385–4391.
34
35 [10] Y. Iwasa, H. Fudo, Y. Yatsu, T. Mitani, H. Kataura, Y. Achiba, Phase
36 stability of doped carbon nanotubes, *Synthetic Metals* 121 (2001) 1203–
37 1204.
38
39 [11] C. Bower, S. Suzuki, K. Tanigaki, O. Zhou, Synthesis and structure of
40 pristine and alkali-metal-intercalated single-walled carbon nanotubes,
41 *Appl. Phys. A - Mater.* 67 (1998) 47–52.
42
43 [12] S. Niyogi, M. A. Hamon, H. Hu, B. Zhao, P. Bhomwik, R. Sen, M. E.
44 Itkis, R. C. Haddon, Chemistry of single-walled carbon nanotubes, *Acc*
45 *Chem. Res.* 35 (2002) 1105–1113.
46
47
48
49
50
51
52
53
54
55
56
57
58
59
60
61
62
63
64
65

- 1
2
3
4
5 [13] A. Kukovecz, T. Pichler, R. Pfeiffer, C. Kramberger, H. Kuzmany, Di-
6 ameter selective doping of single wall carbon nanotubes, *Phys. Chem.*
7 *Chem. Phys.* 5 (2003) 582–587.
8
9 [14] L. Henrard, E. Hernandez, P. Bernier, A. Rubio, Van der waals inter-
10 action in nanotube bundles: consequences on vibrational modes, *Phys.*
11 *Rev. B* 60 (1999) R8521–R8524.
12
13 [15] X. Liu, T. Pichler, M. Knupfer, J. Fink, Electronic and optical properties
14 of alkali-metal-intercalated single-wall carbon nanotubes, *Phys. Rev. B*
15 67 (2003) 125403–1–8.
16
17 [16] K. Tompa, P. Banki, M. Bokor, G. Lasanda, L. Vasaros, Diffusible and
18 residual hydrogen in amorphous Ni(Cu)-Zr-H alloys, *J. Alloys Comp.*
19 350 (2003) 52–55.
20
21 [17] Z. C. Wu, Z. H. Chen, X. Du, J. Logan, J. Sippel, M. Nikolou, K. Ka-
22 marás, J. R. Reynolds, D. B. Tanner, A. F. Hebard, A. G. Rinzler, Trans-
23 parent, conductive carbon nanotube films, *Science* 305 (2004) 1273–
24 1276.
25
26 [18] Á. Pekker, F. Borondics, K. Kamarás, A. G. Rinzler, D. B. Tanner, Cal-
27 culation of optical constants from carbon nanotube transmission spectra,
28 *Phys. Stat. Sol. (b)* 243 (2006) 3485–3488.
29
30 [19] Á. Pekker, K. Kamarás, Wide-range optical studies on various single-
31 walled carbon nanotubes: origin of the low-energy gap, *Phys. Rev. B* 84
32 (2011) 075475–1–8.
33
34 [20] R. Graupner, J. Abraham, D. Wunderlich, A. Vencelová, P. Lauffer,
35 J. Röhr, M. Hundhausen, L. Ley, A. Hirsch, Nucleophilic - alkylation
36 - reoxydation: a functionalization sequence for single-wall carbon nan-
37 otubes, *J. Am. Chem. Soc.* 128 (2006) 6683–6689.
38
39 [21] M. Müller, R. Meinke, J. Maultzsch, Z. Syrgiannis, F. Hauke,
40 A. Pekker, K. Kamarás, A. Hirsch, C. Thomsen, Electronic prop-
41 erties of propylamine-functionalized single-walled carbon nanotubes,
42 *ChemPhysChem* 11 (2010) 2444–2448.
43
44 [22] S. Reich, C. Thomsen, J. Maultzsch, *Carbon Nanotubes: Basic Concepts*
45 and Physical Principles, Wiley-VCH, Weinheim, 2004.
46
47
48
49
50
51
52
53
54
55
56
57
58
59
60
61
62
63
64
65

- 1
2
3
4
5 [23] N. Bendiab, A. M. Saita, R. Aznar, J. L. Sauvajol, R. Almairac, I. Mire-
6 beau, G. Andre, Rubidium localization in single-walled carbon nanotube
7 bundles: structural study, *Phys. Rev. B* 78 (2008) 104108–1–10.
8
9 [24] E. C. T. Harley, L. E. McNeil, The effect of large SWNT diameter dis-
10 tribution on cesium intercalation, *Journal of Physics and Chemistry of*
11 *Solids* 65 (2004) 1711–1718.
12
13 [25] Á. Pekker, D. Wunderlich, K. Kamarás, A. Hirsch, Diameter selectivity
14 of nanotube sidewall functionalization probed by optical spectroscopy,
15 *Phys. Stat. Sol. (b)* 245 (2008) 1954–1956.
16
17 [26] K. Németh, A. Pekker, F. Borondics, E. Jakab, N. M. Nemes, K. Ka-
18 marás, S. Pekker, Investigation of hydrogenated hipco nanotubes by
19 infrared spectroscopy, *Phys. Stat. Sol. (b)* 247 (2010) 2855–2858.
20
21 [27] T. Pichler, M. Sing, M. Knupfer, M. S. Golden, J. Fink, Potassium in-
22 tercalated bundles of single-wall carbon nanotubes: electronic structure
23 and optical properties, *Solid State Commun.* 109 (1999) 721–726.
24
25
26
27
28
29
30
31
32
33
34
35
36
37
38
39
40
41
42
43
44
45
46
47
48
49
50
51
52
53
54
55
56
57
58
59
60
61
62
63
64
65